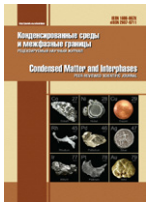

ISSN 1606-867X (Print)
ISSN 2687-0711 (Online)
Condensed Matter and Interphases
Kondensirovannye Sredy i Mezhfaznye Granitsy
https://journals.vsu.ru/kcmf/

Original articles

Research article
https://doi.org/10.17308/kcmf.2026.28/13588

Microstructural and hydrophilic properties of acrylonitrile-butadiene-styrene copolymer ABS samples with different 3D-printed patterns

A. S. Lenshin[1], V. E. Frolova[1], V. A. Makagonov[2], A. K. Pelagina[1], E. P. Domashevskaya[1]✉

[1]*Voronezh State University,*
1, Universitetskaya pl., Voronezh 394018, Russian Federation

[2]*Voronezh State Technical University,*
14, Moskovsky pr., Voronezh 94026, Russian Federation

Abstract

Objectives: The aim of this study is to investigate the influence of different 3D printing patterns, under identical thermal and mechanical parameters of the 3D printing process itself, on the microstructural and hydrophilic properties of amorphous ABS copolymer samples printed with five different 3D printing patterns by sequentially depositing layers using FDM (Fused Deposition Modeling).

Conclusions: The results of studying the printed samples using SEM, X-ray diffraction, IR spectroscopy, and contact angle measurements showed that the combination of thermal and mechanical effects during 3D printing in the studied extrusion mode does not cause noticeable orientation of the polymer chains of the original amorphous ABS copolymer, does not disrupt its intrastructural chemical bonds, and the surface of all printed samples with five different patterns is hydrophilic. Moreover, the printed sample with the most complex geometry is the 1_Hilbert pattern, which has the most distorted morphology and surface defects and exhibits the highest contact angle ($\varphi = 67^{o}$), exceeding the corresponding values in samples with other patterns ($\varphi \approx 60^{o}$) by ~10 %, and has a hydrophilic surface.

Keywords: Acrylonitrile-butadiene-styrene copolymer ABS, Various 3D-printed patterns, Printed samples, Surface morphology, Amorphous state, IR spectra, Contact angles, Hydrophilic surface.

Funding: This work was supported in part by the Ministry of Education and Science of the Russian Federation under a state assignment for universities in the field of scientific activity, project no. FZGU-2026-0009, and the Advanced Engineering School of VSU.

For citation: Lenshin A. S., Frolova V. E., Makagonov V. A., Pelagina A. K., Domashevskaya E. P. Microstructural and hydrophilic properties of acrylonitrile-butadiene-styrene copolymer ABS samples with different 3D-printed pattern designs. *Condensed Matter and Interphases*. 2026;28(1): 69–80. https://doi.org/10.17308/kcmf.2026.28/13588

Для цитирования: Леньшин А. С., Фролова В. Е., Макагонов В. А., Пелагина А. К., Домашевская Э. П. Микроструктурные и гидрофильные свойства образцов из сополимера акрилонитрил-бутадиен-стирол ABS с различными модельными рисунками 3D-печати. *Конденсированные среды и межфазные границы*. 2026;28(1): 69–80. https://doi.org/10.17308/kcmf.2026.28/13588

✉ Evelina P. Domashevskaya, e-mail: ftt@phys.vsu.ru

1. Introduction

Thermoplastic polymers play an important role in various engineering fields due to their excellent functional and technological properties. Along with other thermoplastics, acrylonitrile-butadiene-styrene copolymer (ABS) is widely used as a structural material. ABS consists of varying amounts of polyacrylonitrile (15–30 %), polybutadiene (5–35 %), and polystyrene (40–60 %) and is widely used in the aerospace and defense industries, automotive manufacturing, and in electrical, telecommunications, and computer technologies [1]. The advantages of ABS copolymer also include the ability to manufacture various products with matte and mirror-like surfaces. ABS exhibits good impact resistance, toughness, rigidity, heat resistance, elasticity, and environmental friendliness. It is tolerant to moisture, inorganic acids and salts, solvents, lubricating oils, and alkalis. A significant advantage of ABS thermoplastic is its recyclability. The chemical formula of the acrylonitrile-butadiene-styrene (ABS) copolymer consists of three parts: $(C_8H_8)_x \cdot (C_4H_6)_y \cdot (C_3H_3N)_z$ [2].

The structural formula of the ABS copolymer [3, 4] is shown in Fig. 1.

The melting point of the ABS copolymer ranges from 220 °C to 260 °C, but it begins to soften at approximately 105 °C. Different grades of ABS may have slightly different melting points, but this range is generally typical. It should also be noted that the glass transition of the ABS copolymer occurs in the temperature range of approximately 60÷65 °C.

ABS products are recommended for use in temperatures ranging from –20 to 80 °C, as their mechanical properties vary with temperature [3].

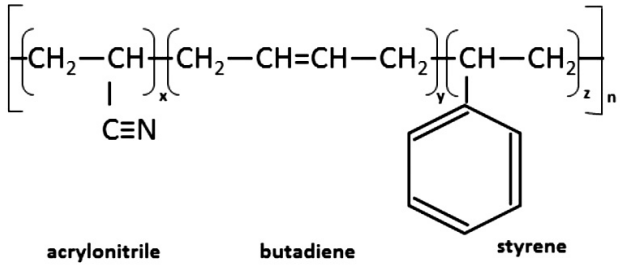

Fig. 1. Structural formula of the acrylonitrile-butadiene-styrene (ABS) copolymer [3, 4]

However, the material easily withstands short-term exposure to temperatures up to +100°C, as well as long-term heating at +75÷80 °C. The rigidity, mechanical strength, and durability of ABS significantly exceed those of high-impact polystyrene and other polymers. To increase impact resistance, viscosity, and heat resistance, the ratio of polybutadiene, polystyrene, and polyacrylonitrile copolymers in ABS can be varied, allowing for the production of different grades of ABS by varying the component proportions [3].

The properties of ABS products also depend to some extent on the conditions under which the material is processed into the final object. For example, high-temperature molding improves the gloss and heat resistance of products, while the highest impact resistance is achieved with low-temperature molding. Fibers (usually fiberglass) and additives can be blended with resin granules to impart strength to the final product and increase its maximum operating temperature. Pigments can also be added to ABS, as its natural color ranges from translucent ivory to white. Additives are also used to protect against ultraviolet radiation [2].

ABS copolymers are resistant to aqueous acids, alkalis, concentrated hydrochloric and phosphoric acids, as well as animal, vegetable, and mineral oils. They are soluble in esters, acetone, chloroform, and ethylene dichloromethane, and exhibit low resistance to chlorinated solvents, alcohols, and aldehydes [2].

Although ABS thermoplastics are primarily used in mechanical applications, they also exhibits electrical properties that are quite stable over a wide frequency range. Temperature and humidity have virtually no effect on these properties within the permissible operating temperature range [4]. However, when exposed to high temperatures, such as during wood combustion, ABS plastics are highly flammable. They melt and then boil, after which the vapors turn into an intense hot flame, releasing toxic decomposition products. The toxicity of ABS thermoplastics are characterized in [5].

Of particular importance to modern materials science is the fact that, along with other thermoplastics, acrylonitrile butadiene styrene is a common material used in 3D printers [6] as ABS

filament because it is inexpensive, durable, highly stable, and can be post-processed in various ways, including sanding, painting, gluing, casting, and chemical smoothing.

It is known [6] that ABS deforms when used in 3D printing due to shrinkage that occurs during cooling during the printing process. However, shrinkage can be reduced by printing samples on a heated print surface, using glue to ensure good adhesion of the first layer of the print to the print surface, or printing with edges/rafts at the base of the print to improve adhesion to the print surface [6].

The aim of this study is to investigate the influence of different 3D printing patterns under identical thermal and mechanical parameters of the 3D printing process on the microstructural and hydrophilic properties of ABS copolymer samples printed with five different 3D printing patterns by sequentially depositing layers using Fused Deposition Modeling (FDM). Structural and optical characterization methods enable rapid characterization and comparison of acrylonitrile-butadiene-styrene polymer compounds [7]. Furthermore, infrared calibration curves are extremely useful in analyzing the composition of ABS plastic. Analyses based on this method provide information that can be used to predict the physical properties of the formed plastic [7–12].

Therefore, to achieve our goal of studying the influence of the 3D printing process on the microstructural and hydrophilic properties of ABS-printed samples, we used scanning electron microscopy (SEM), X-ray diffraction (XRD), IR spectroscopy, and contact angle measurements to determine surface wettability.

The prerequisites for studying the influence of different patterns on the properties of ABS samples in this work are the differences in the chemical formula of ABS, and especially its structural formula (with a long repeat period), from the corresponding parameters of two other thermoplastics, PETG and PLA, and the observed tendency for the contact angle to increase (hydrophilicity to decrease) in printed samples with the most complex pattern, i.e., 1_Hilbert: up to 4 % [13] in the PETG sample and up to 10 % [14] in the PLA sample. We previously conducted similar studies of the effect of the 3D printing process on the microstructural and hydrophilic properties of samples with the same pattern printed from two other thermoplastic polymers: polyethylene terephthalate-glycol (PETG) and polylactic acid (PLA). Therefore, when discussing the results obtained in this study, we will compare them with similar results for two other polymers published in our papers [13] and [14].

Despite the presence of papers in modern scientific journals devoted to modeling the properties, computer design, and improvement of polymer models and computer programs, we did not find any studies on the possible influence of pattern designs on polymer properties. Only one theoretical study on modeling the influence of the structure of an amorphous-crystalline polymer on its deformation properties [15] showed that the deformation characteristics of the polymer depend significantly on the relative positions of the crystalline and amorphous phases of the polymer in accordance with the five structural models considered: 1 – ideal phase mixing; 2 – square lattice of the crystalline phase; 3 – square lattice of the amorphous phase; 4 – staggered phase arrangement; 5 – random phase arrangement.

However, in the theoretical modeling conducted in [15], deformation and structural rearrangements of the amorphous phase were not taken into account. Whereas in the following sections of the article, we will show that the polymer we studied, both in the initial ABS filament state and in the printed samples, contains only one amorphous phase. It is this circumstance that determines the novelty and relevance of our experimental study of the possible influence of different geometry of the 3D printing model pattern on the microstructural and hydrophilic properties of ABS printed samples with five different model patterns.

2. Experimental. Research objects and methods

The test specimens were made from colorless MAKO 1.75 Natural ABS Filament with a diameter of 1.75 mm using the Fused Deposition Modeling (FDM) method on a Hercules Original 3D printer at an extruder temperature of 240 °C and a

power of 500 W. Table 1 presents the 3D printer parameters used to print specimens with five different patterns. Using the parameters listed in Table 1, five cylindrical specimens with different 3D patterns were printed.

Fig. 2 shows the five types of patterns studied. The patterns shown in Fig. 2 were taken from the Prusa Slicer modeling software. After constructing five models with different 3D patterns, five samples with five different 3D patterns (1_Hilbert, 2_Concentric, 3_Archimedian, 4_Rectilinear, 5_Octagram) were printed from these models.

The printed colorless samples have the same cylindrical shape with a diameter of 20 mm and a thickness of 5 mm. Along with the printed samples, the original filamentary acrylonitrile-butadiene-styrene (ABS filament) sample was studied, so the next section presents the results of the microstructural properties of the six samples.

Scanning electron microscopy (SEM) of the surfaces of the five printed samples with different patterns was performed on a JSM 6510LV scanning electron microscope at the VSU Center for Collective Use. To obtain better contrast in the SEM micrographs, surface morphology studies of the printed samples were performed on the surfaces of samples coated with a very thin gold layer (a few nanometers thick) at various magnifications of ×40, ×1000, and ×5000.

Table 1. 3D printing parameters on a Hercules Original printer

3D Printing Parameter	Value
Value layer thickness / extruder nozzle diameter	0.8 mm
Filling density	20 %
Filling speed	50 mm/s
Filling model patterns	5 types
Sample thickness	5.0 mm
Extruder nozzle temperature	240 °C

X-ray diffraction (XRD) analysis of the printed samples and the original ABS filament was performed at the Voronezh State Technical University using a BRUCKER D2 Phaser diffractometer (with a copper anode), at a high voltage of U = 30 kV and anode current of I = 10 mA in the Bragg angle range $2\theta = 5–80^{\circ}$.

IR spectroscopy is a universal method for obtaining information on the molecular structure of substances and allows one to determine the nature of atomic groups, the nature of chemical bonds, and their changes under external conditions [16, 17]. The molecular structures of the ABS filament and five 3D-printed samples with different patterns were studied by measuring IR transmission spectra on a Brucker Vertex 70 FTIR spectrometer at the Voronezh State University Center for Collective Use in the range of 400–4000 cm^{-1}.

The surface wettability of five flat 3D-printed samples with different patterns was determined using a unique contact angle measuring setup (Fig. 3), which we manufactured on a Hercules Original 3D printer. The setup consists of a stand with a sample holder on which a flat sample is placed. A droplet meter is placed on the stand, which creates droplets on the sample surface to measure the contact angle. A webcam is mounted opposite the stand containing the sample, displaying the droplet image on the screen. The contact angle of the sample, φ^{o}, is measured using the Pic-pic graphics editing program.

A liquid droplet on the surface of a solid, depending on the nature of the sample, the liquid itself, and the environment in which it is located,

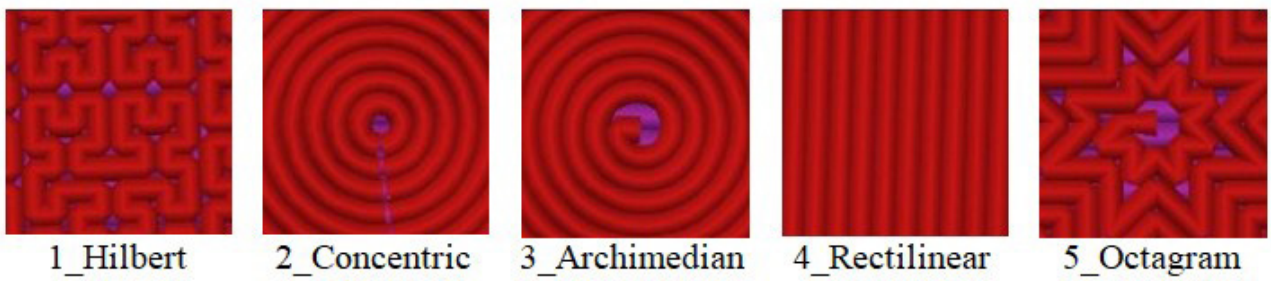

Fig. 2. Five types of 3D printed patterns on ABS (acrylonitrile butadiene styrene) polymer samples: 1_Hilbert, 2_Concentric, 3_Archimedian, 4_Rectilinear, 5_Octagram

can spread completely or partially, taking on the appearance shown in Fig. 4. The angle φ between the tangent to the droplet surface and the surface of the solid, measured toward the droplet surface, is called the contact angle φ° [18, 19]. Only those liquids that lower the surface tension of the solid at the interface with air (φ < 90°) wet a solid surface. Solid surfaces wetted by water are called hydrophilic. For hydrophobic surfaces, the contact angle φ > 90°.

Using the methods listed above, we answer questions about the influence of the technological process and the geometry of the pattern on the surface morphology of printed samples, their microstructure, and surface wettability. Answers to these questions are contained in the following sections of the article.

3. Results and discussion

3.1. Sample morphology based on scanning electron microscopy (SEM) data

Fig. 5 shows SEM micrographs obtained at different magnifications of ×40, ×1000, and ×5000 for five samples printed from ABS filament with different patterns.

The SEM results for the five printed samples, compared with the model types in Fig. 2, show that the polymer fills the sample volumes during 3D printing not as continuous smooth layers, but as layers with a morphology structured more or less in accordance with its pattern and a low filling density of approximately 20 %.

Sample 1_Hilbert, with the most complex pattern, exhibits the greatest distortion of its geometry during 3D printing. For example, in Fig. 2, the 1_Hilbert pattern shows only right angles in its complex geometry, whereas the SEM micrograph of the sample printed using this model (Fig. 5, 1.1_Hilbert X40) shows no undistorted rectangular shapes.

The micrographs of samples with patterns 4_Rectilinear and 5_Octagram most accurately and contrastingly reflect the geometry of the 3D printed pattern.

A comparison of Fig. 5 and Fig. 2 shows that the surface micrographs of two samples with similar circular patterns, 2_Concentric and 3_Archimedian (Fig. 2), adequately reflect the curvilinear geometry of the circular arc in the two printed samples with these patterns to a more or less equal degree (Fig. 5).

3.2. X-ray diffraction of the original ABS filament sample and printed ABS copolymer samples

The diffractograms of five printed samples with different 3D patterns and the original ABS polymer filament are shown in Fig. 6. The XRD results, obtained in the Bragg angle range 2θ = 5–80°, showed that all five samples with different 3D patterns made of amorphous ABS polymer filament are indeed amorphous, just like the original ABS filament itself. All diffractograms contain two broad bands of diffraction reflections:

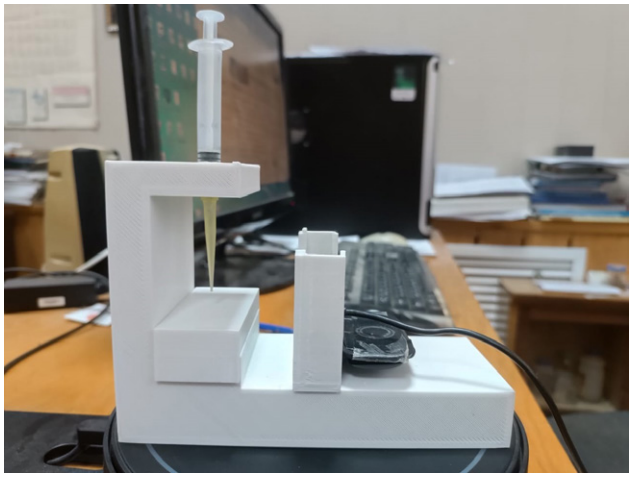

Fig. 3. The original setup for measurement of the contact angle, printed on a Hercules Original 3D printer

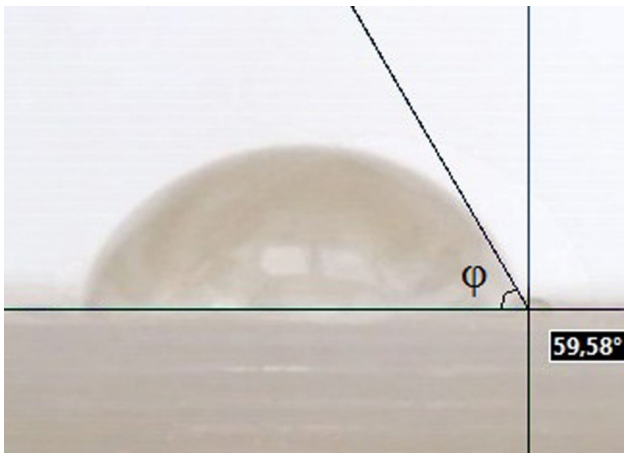

Fig. 4. Contact angle φ on the hydrophilic surface of one of the printed samples with the 3_Archimedean pattern

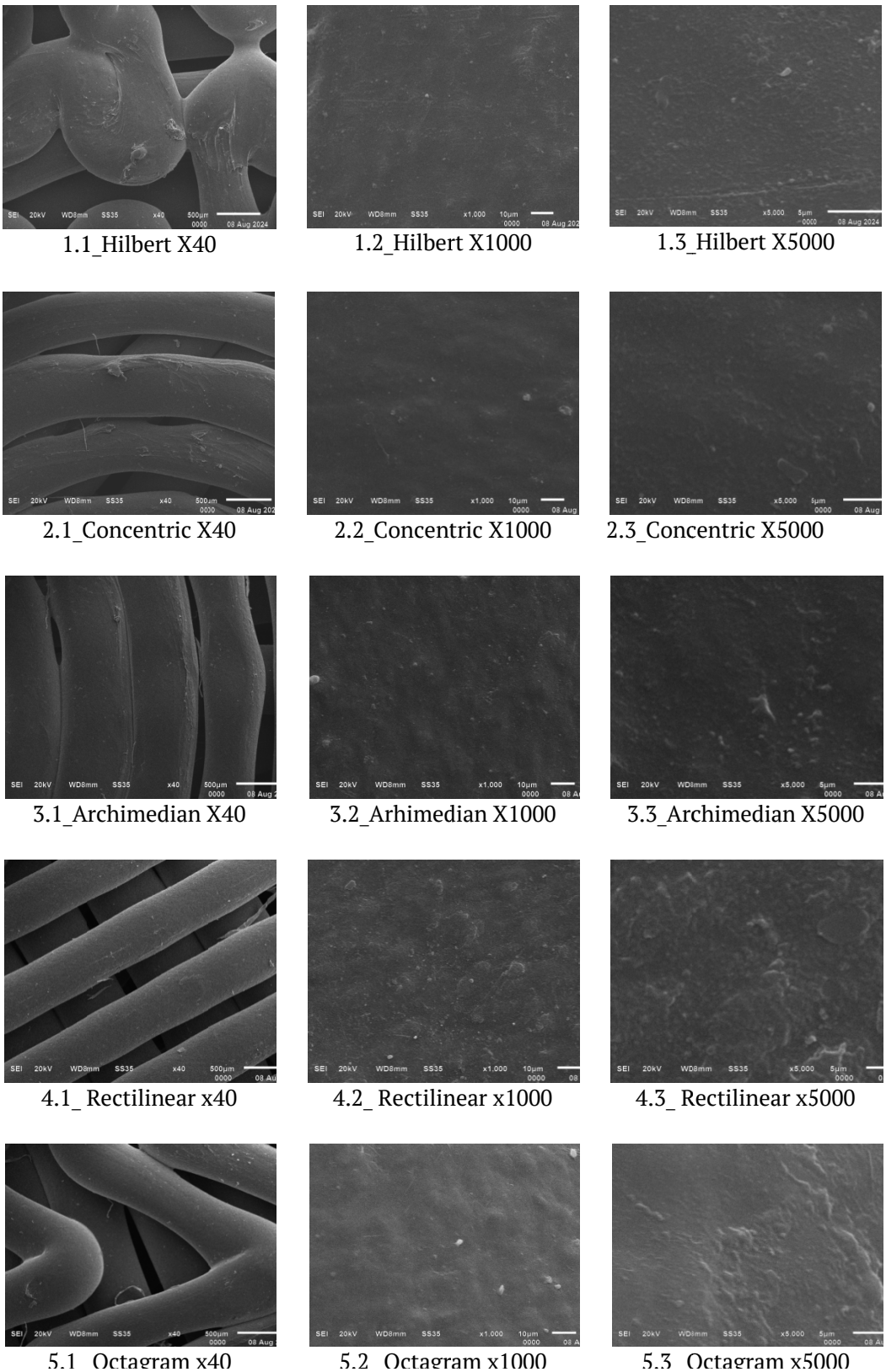

Fig. 5. SEM micrographs at ×40, ×1000, and ×5000 magnification for ABS samples with different patterns: 1_Hilbert, 2_Concentric, 3_Archimedian, 4_Rectilinear, 5_Octagram

a main band with a maximum near 2θ ≈ 20° and a shoulder at 2θ ≈ 12°, and a second, low-intensity band with a maximum at 2θ ≈ 43°.

It should be noted that the diffraction band shapes we obtained are in good agreement with the X-ray structural data reported for ABS in the literature [9–12]. Furthermore, a comparison of our X-ray structural data for ABS with our results for two other polymers, PETG [13] and PLA [14], indicates some differences in the shape and position of the X-ray diffraction bands of the original amorphous filamentary samples and different degrees of influence of the 3D printing process on the microstructural properties of samples printed from three different polymers.

Thus, in our previous work we established that the differences in the diffraction patterns of printed PETG samples from the diffraction pattern of the original PETG filament are due to the greater ordering of the polymer chains in the printed samples with different patterns, which occurs under thermal and mechanical influences on the original filament sample during 3D printing and is manifested in an increase by an order of magnitude in the relative intensity of the main diffraction maximum of the amorphous PETG polymer in all printed samples compared to the original amorphous filament [13].

We discovered even greater differences between the diffraction patterns of the printed samples and the diffraction pattern of the original amorphous filament during 3D printing from the PLA polymer. These differences were due to partial crystallization of the initially misoriented polymer chains of amorphous PLA, resulting in the formation of an orthorhombic α-Poly(L-lactide) phase, which occurs in the extruder under thermal and mechanical influences on the original amorphous filamentary sample [14].

Moreover, the most noticeable crystallization with the formation of the orthorhombic α-phase of PLA occurs in the printed samples with the 3_Archimedian and 5_Octagram patterns, which the extruder produces continuously within each layer during continuous layer-by-layer accumulation of the total sample thickness of 5 mm.

Thus, a comparative analysis of the shape and relative intensity of X-ray diffraction patterns of samples made from three different thermoplastic polymers indicates the greatest stability of the amorphous microstructure of ABS copolymer with respect to thermal and mechanical influences during printing on a Hercules Original 3D printer and the preservation of the original amorphous state in all printed samples across the five model patterns.

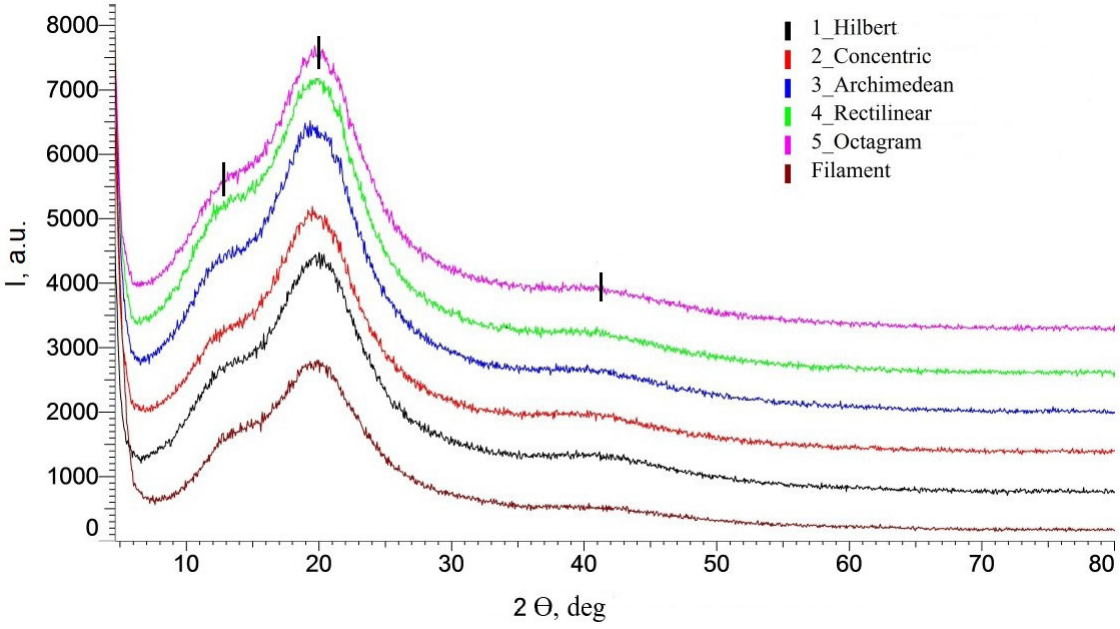

Fig. 6. X-ray diffractograms obtained in the Bragg angle range 2θ = 5–80° for the original filament and five samples printed from ABS filament with different patterns: 1_Hilbert, 2_Concentric, 3_Archimedian, 4_Rectilinear, 5_Octagram

3.3. IR spectra of the original ABS filaments and printed ABS copolymer samples

IR spectroscopy is a non-destructive optical method used to solve specific problems, including determining the fundamental characteristics of a molecule, quantitatively analyzing known phases in a substance, identifying chemical compounds, and elucidating their structure [18–20]. This optical method is based on measuring the intensity of infrared (IR) radiation absorbed or reflected by a given material. This intensity is associated with vibrational and rotational oscillations of molecular fragments and manifests itself in the intensity distribution in absorption bands depending on the wavelength (λ) or its reciprocal, which is known as the wavenumber (ν). Fig. 7 shows the IR transmission spectra for the original filament sample (ABS Filament) and five 3D-printed samples with different pattern designs.

Table 2 presents the identification of all vibration modes of ABS molecular fragments in the original filament (ABS filament) and the five printed ABS samples.

The IR spectroscopy results show that the wavenumbers and relative intensities of the absorption bands for all five printed samples with different patterns are similar and coincide, within the measurement accuracy, with the corresponding values of the main absorption bands of the original ABS filament used in 3D printing our samples and with literature data for ABS copolymer [9–11]. This means that its intrastructural chemical bonds are not subject to mechanical and thermal influences during 3D printing, just as its amorphous microstructure, which we discussed above based on XRD data, is not subject to these influences.

3.4. Surface wettability of printed ABS specimens with different patterns

Surface wettability is a manifestation of intermolecular interactions at the interface of

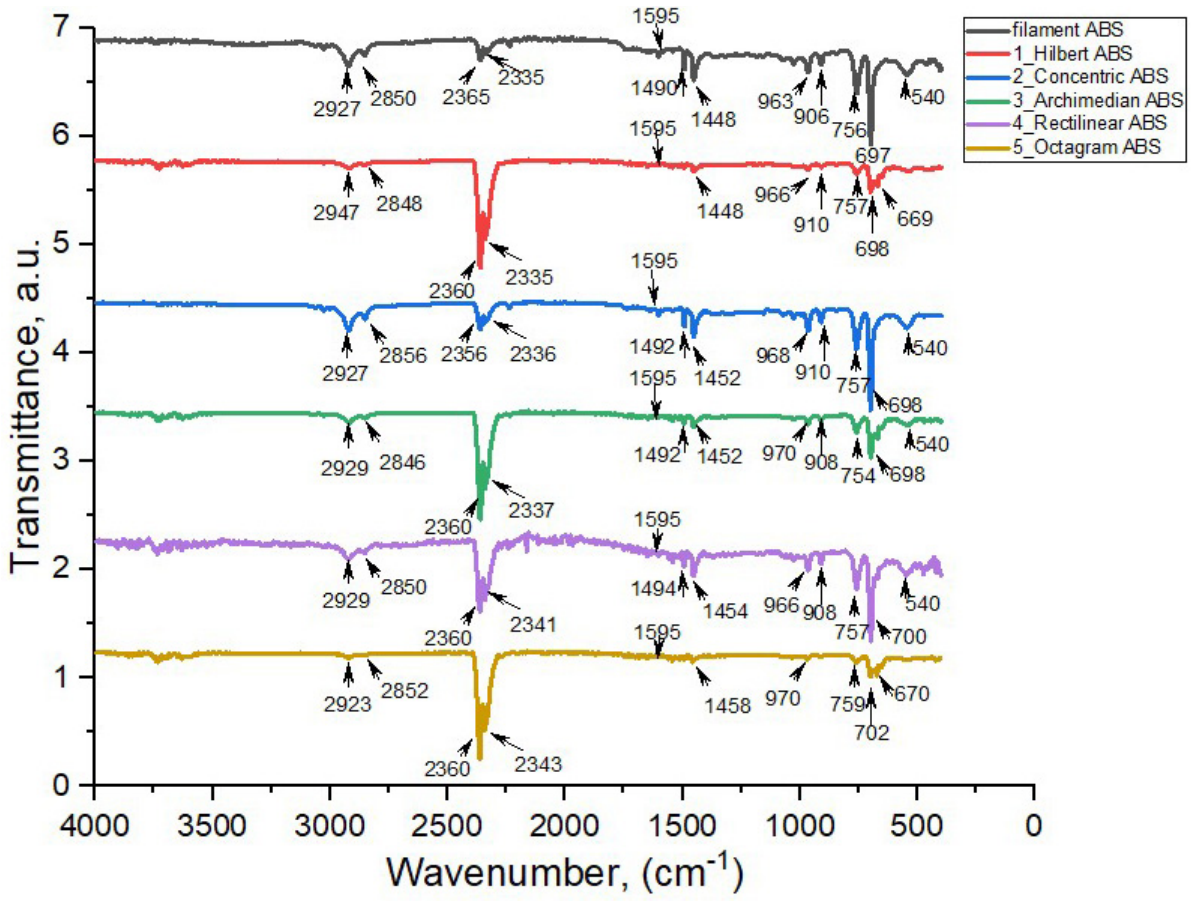

Fig. 7. IR transmission spectra from the original ABS filament and five printed samples with different patterns.

Таблица 2. Моды колебаний ИК-спектров исходного нитевидного образца Filament ABS и напечатанных образцов с различными модельными рисунками

Identification of vibration modes	Vibration modes ABS, cm^{-1}						
	Filament ABS	1_Hilbert	2_Concentric	3_Archimedian	4_Rectilinear	5_Octagram	ABS [references]
Nitrile	540	539	540	540	540	539	539 [10]
C-H out of plane bond	697	700	698	698	700	702	696 [10]
=C-H out of plane bond	756	757	757	754	757	759	757 [10]
C-H bending for H atoms attached to alkene carbons in butadiene	906 963	910 966	910 968	908 970	908 966	– 970	911 [12] 967 [12] 955 [10]
C-H bending asymmetry Scissor mode of CH_2 groups	1448	1448	1452	1452	1454	1458	1453 [12] 1450 [10]
C-H bend asymmetry Aromatic ring in styrene	1490	–	1492	1492	1494	–	1494 [11] 1492 [10]
C=C (styrene)	1595	1595	1595	1595	1595	1595	1589[10]
Bending of the N–C bond in acrylonitrile	2365 2335	2360 2335	2356 2336	2360 2337	2360 2341	2360 2343	2356 [10] 2238 [12]
Aromatic and aliphatic C-H stretching modes	2850 2927	2848 2947	2856 2927	2846 2929	2850 2929	2852 2923	2800–3200 [12] 2922 [10]

three phases: solid, liquid, and gas, resulting in a liquid spreading across the surface of a solid [19–21]. Since contact angle measurements are only performed on flat specimens, this section presents wettability results for five printed specimens.

Fig. 8 shows photographs of droplets taken using the original contact angle measurement setup on the surface of five printed ABS specimens with different 3D printed patterns. Contact angle measurements of water droplets on the surface of the specimens were taken at six points for each specimen, which were then averaged to an accuracy of one degree.

Table 3 presents the average contact angle values for the five printed specimens.

A comparative analysis of the surface contact angles of the samples in Table 3 and Fig. 8 shows that the average contact angles for all printed samples vary within the range of $\varphi = 59 \div 67°$. The large deviation of all average contact angle values toward smaller values relative to a right angle of 90° indicates that the surfaces of all five printed ABS copolymer samples with different patterns are hydrophilic.

Moreover, sample 1_Hilbert, with the most complex pattern geometry and the most distorted morphology, exhibits the highest average contact angle of $\varphi = 67°$, i.e., it is less hydrophilic than the others.

Four samples with other patterns, whose surface micrographs in Fig. 5 reflect the geometry of their pattern to a less distorted degree, have similar contact angles of approximately $\varphi \approx 60°$. Thus, one can see some influence of the more complex geometry of the 1_Hilbert pattern in the 3D-printed sample, manifested in the distorted surface morphology in Fig. 5, also on the wettability of its surface, towards a decrease in hydrophilicity (Table 3).

In printed samples with the same patterns from another thermoplastic polymer, polylactide (PLA), we previously found [14] that the sample with the same 1_Hilbert pattern geometry also exhibits the highest contact angle $\varphi = 59°$ compared to other samples ($\varphi = 50–55°$).

Since the wettability of a solid surface is a manifestation of intermolecular interactions at the interface between a liquid and a solid surface, it can be assumed that one mechanism for this interaction

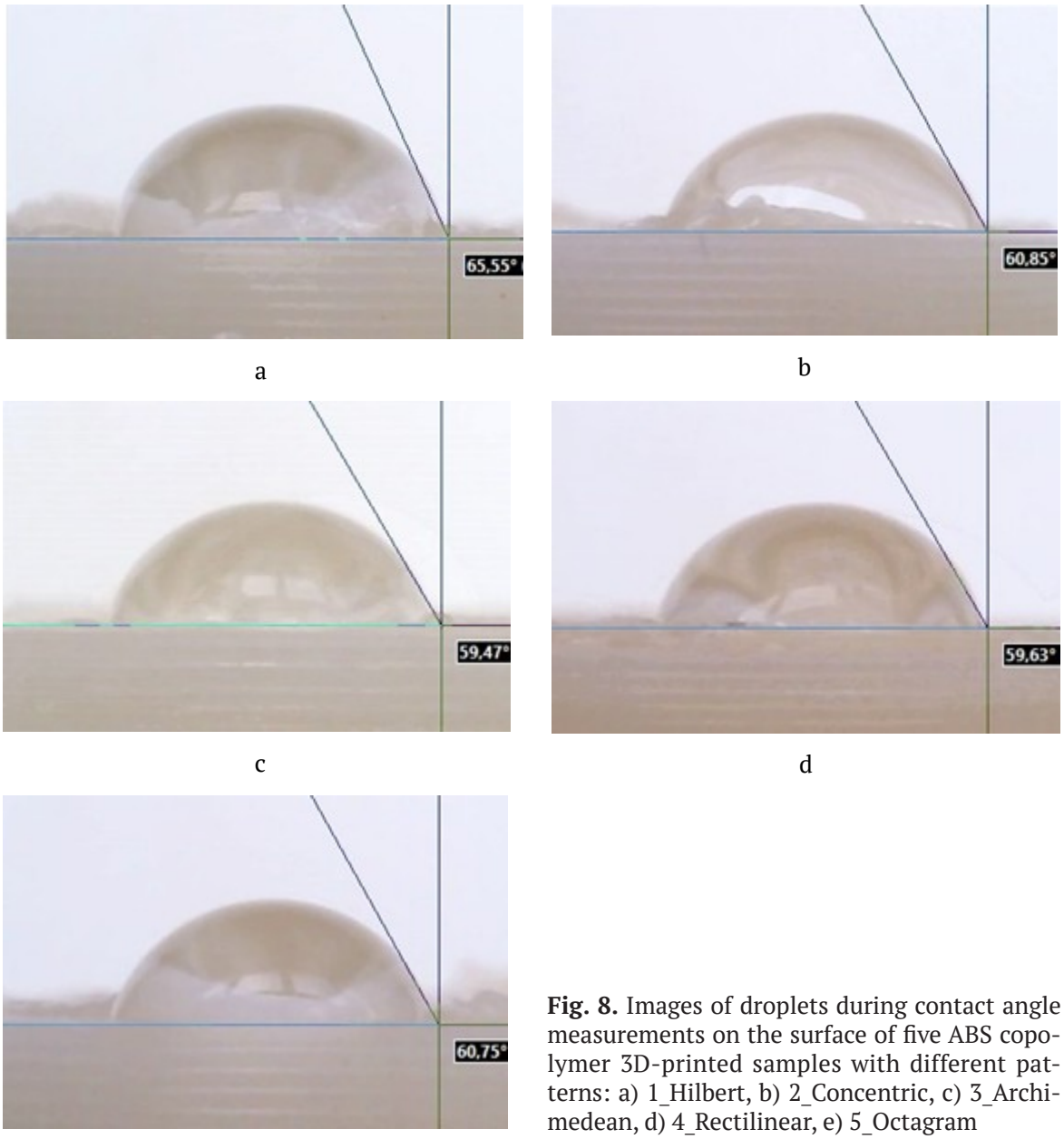

Fig. 8. Images of droplets during contact angle measurements on the surface of five ABS copolymer 3D-printed samples with different patterns: a) 1_Hilbert, b) 2_Concentric, c) 3_Archimedean, d) 4_Rectilinear, e) 5_Octagram

Table 3. Average contact angle values (φ°) on the surface of ABS samples with different 3D-printed patterns

Sample number and model pattern type	Average values of wetting edge angle φ°
1_Hilbert	67
2_Concentric	60
3_Archimedian	63
4_Rectilinear	59
5_Octagram	59

may be the participation of the polar groups of the ABS polymer in the formation of hydrogen bonds with water molecules on the surface of all five samples. This leads to a significant decrease in the contact angles relative to 90° and the hydrophilicity of all ABS-printed samples. Moreover, sample 1_Hilbert, with the most complex pattern, the most distorted morphology, and surface defects, exhibits the highest average contact angle (φ = 67°), i.e., it is less hydrophilic due to the greatest difficulties in forming hydrogen bonds with water molecules on its surface.

3. Conclusion

The results obtained in studying the effect of the 3D printing process on the microstructural and hydrophilic properties of ABS copolymer samples obtained by sequentially depositing copolymer layers using the FDM method on a Hercules Original 3D printer with five different model patterns showed:

– All five samples, printed with different 3D patterns from amorphous ABS filament, retain the original amorphous state of the filamentous sample.

– A comparative analysis of the shape and relative intensity of the XRD diffraction patterns of the ABS samples with the X-ray diffraction data of two other polymers, PETG and PLA, indicates the greatest resistance of the amorphous microstructure of the ABS copolymer under study to thermal and mechanical stress during 3D printing compared to the other two polymers.

– The intrastructural chemical bonds of ABS are also not susceptible to the mechanical and thermal effects of the 3D printing process, and therefore the wavenumbers and relative intensities of the IR spectral bands of all five printed samples with different pattern designs have similar values, which coincide, within the measurement accuracy, with the corresponding values of the main absorption bands of the original ABS filament and with literature data.

– The average contact angles of the printed ABS copolymer samples with five different patterns vary within the range of $\varphi = 59 \div 67°$, significantly less than a right angle, and therefore the surfaces of all printed samples are hydrophilic.

– The printed sample with the most complex geometry, the most distorted morphology, and the most surface defects, the 1_Hilbert pattern, exhibits the highest contact angle ($\varphi = 67°$), exceeding the corresponding values in samples with other pattern designs ($\varphi \approx 60°$) by ~10 %. It also has a less hydrophilic surface due to a possible reduction in hydrogen bonds with water molecules on its more defective surface.

Thus, the obtained results demonstrate that the thermal and mechanical effects of 3D printing in the studied extrusion mode do not cause a noticeable orientation of the polymer chains of the original amorphous ABS copolymer, do not disrupt its intrastructural chemical bonds, and the surfaces of the printed samples with five different pattern designs are hydrophilic.

Author contributions

The authors contributed equally to this article.

Conflict of interests

The authors declare that they have no known competing financial interests or personal relationships that could have influenced the work reported in this paper.

References

1. Kumar R. M., Rajini N. T., Kumar S. M., Mayandi K., Siengchin S., Ismail S. O. Thermal and structural characterization of acrylonitrile butadiene sstyrene (ABS) copolymer blended with polytetrafluoroethylene (PTFE) particulate composite. *Materials Research Express.* 2019;6(8): 085330. https://doi.org/10.1088/2053-1591/ab250f

2. Peters E. N. *Plastics: thermoplastics, thermosets, and elastomers*. Handbook of Materials Selection. Kutz M. (ed.). New York: John Wiley & Sons, Inc.; 2002. p. 363–365. https://doi.org/10.1002/9780470172551.ch11

3. Kutnjak-Mravlincic S., Sutlovic A., Glogar M. I., Ercegovic Ražic S., Godec D. Innovative development of batch dyed 3D printed acrylonitrile-butadiene-styrene objects. *Molecules.* 2021;26: 6637. https://doi.org/10.3390/molecules26216637

4. Kulich D. M., Gaggar S. K., Lowry V., Stepien R. Acrylonitrile–butadiene–styrene polymers. In: *Encyclopedia of Polymer Science and Technology.* Hoboken, NJ, USA: John Wiley & Sons; 2001. p. 174–201. https://doi.org/10.1002/0471440264.pst011

5. Mukhamedyanov E. R., Orlova N. Yu. Toxicity of non-engineering plastics during extrusion*. *Collection of scientific papers of the All-Russian scientific and practical conference. December 22–23, 2020.* Moscow: NRNU MEPhI; Snezhinsk: SFTI NRNU MEPhI; 2020: 56-59.

6. Harper C. A. *Handbook of plastic and elastomers*. New York: McGraw-Hill; 1997. p. 1–62. ISBN 0070266816

7. Rutkowski J. V., Levin B. C. Acrylonitrile-butadiene-styrene copolymers (ABS): pyrolysis and combustion products and their toxicity- a review of the literature. *Fire and Materials.* 1986;10(3-4): 93–105. https://doi.org/10.1002/fam.810100303

8. Steeman P. A., Meier R. J. The structure of styrene-acrylonitrile/bytadiene polymer studied by 2D-i.r. spectroscopy. *Polymers,* 1997;38(21): 5435–5462. https://doi.org/10.1016/s0032-3861(97)00074-8

9. Bandeira L. C., Campos B. M., Ciuffi K. J., ... Maia I. A. Calcium phosphate coatings by sol-gel on acrylonitrile-butadiene-styrene substrate. *Journal of the Brazilian Chemical Society.* 2017;28(6): 943–949. https://doi.org/10.21577/0103-5053.20160244

10. Boricha A. G., Murthy Z. V. P. Acrylonitrile-butadiene-styrene/chitosan blend membranes: preparation, characterization and performance for the separation of heavy metals. *Journal of Membrane Science.* 2009;339(1): 239–249. https://doi.org/10.1016/j.memsci.2009.04.057

11. Desrousseaux C., Cueff1 R., Aumeran C., ... Sautou V. Fabrication of acrylonitrile-butadiene-styrene nanostructures with anodic alumina oxide templates, characterization and biofilm development test for staphylococcus epidermidis. *PLOS ONE*. 2015;10(8): e0135632. https://doi.org/10.1371/journal.pone.0135632

12. Neher B., Gafur Md. A., Al-Mansur M. A., Bhuiyan Md. M. R., Qadir Md. R., Ahmed F. Investigation of the surface morphology and structural characterization of palm fiber reinforced acrylonitrile butadiene styrene (PF-ABS) composites. *Materials Sciences and Applications,* 2014;5: 378–386. https://doi.org/10.4236/msa.2014.56043

13. Lenshin A. S., Frolova V. E., Ivkov S. S., Domashevskaya E. P. Microstructural and hydrophilic properties of polyethylene terephthalate glycol polymer samples with different 3D printing patterns. *Condensed Matter and Interphases*. 2024;26(1): 78–87. https://doi.org/10.17308/kcmf.2024.26/11810

14. Lenshin A. S., FrolovaV. E., Kannykin S. V., Domashevskaya E. P. Microstructural and hydrophilic properties of polylactide polymer samples with various 3D printing patterns. *Polymers*. 2024;16: 1281. https://doi.org/10.3390/polym16091281

15. Oshmyan V. G., Timan S. A., Shamaev M. Yu. Modeling of ductile failure of polymer blends and composites with account of interface formation. *Polymer Science, Series A*. 2003;45(10): 1011–1018. Available at: https://elibrary.ru/item.asp?id=13425982]

16. Gremlikh G. U. *The language of spectra. Introduction to the interpretation of spectra of organic compounds**. Brooker. Opt.; 2002. 94 p. (in Russ.)

17. Hollas J. M. *Modern Spectroscopy. Fourth Edition*. The Atrium, Southern Gate, Chichester, West Sussex, England: John Wiley & Sons Ltd.; 2004. 452 p.

18. Tolstoy V. P., Chernyshova I. V., Skryshevsky V. A. *Handbook of infrared spectroscopy of ultrathin films*. Hoboken, New Jersey: John Wiley & Sons, Inc.; 2003. 739 p. https://doi.org/10.1002/047123432x

19. Kiselev M. G., Savich V. V., Pavich T. P. Determination of the contact wetting angle on flat surfaces. *Bulletin of BNTU*. 2006;1: 38–41. Available at: https://elibrary.ru/item.asp?id=21398120

20. Elesina V. V. *Wetting angle. Methodical recommendations**. Altai State Technical University named after I. I. Polzunov Publ.; 2019. 22 c. (in Russ.)

21. Pavlov I. N., Rinkevichyus B. S., Tolkachev A. V. A setup for visualizing the evaporation of a liquid drop using the method of frustrated total internal reflection of a laser beam. *Instruments and Experimental Techniques*. 2013;56(2): 242–246. https://doi.org/10.1134/s0020441213020103

** Translated by author of the article*

Information about the authors

Aleksandr S. Lenshin, Dr. Sci. (Phys.–Math.), Leading Researcher, Department of Solid State Physics and Nanostructures, Voronezh State University (Voronezh, Russian Federation).

https://orcid.org/0000-0002-1939-253X
lenshinas@mail.ru

Vera E. Frolova, Cand. Sci. (Phys.–Math.), Associate Professor, Department of Solid State Physics and Nanostructures, Voronezh State University (Voronezh, Russian Federation).

https://orcid.org//0009-0000-2880-8958
ternovaya@phys.vsu.ru

Vladimir A. Makagonov, Cand. Sci. (Phys.–Math.), Associate Professor, Department of Physics, Voronezh State Technical University (Voronezh, Russian Federation).

https://orcid.org/0000-0002-4024-4064
vlad_makagonov@mail.ru

Alexandra K. Pelagina, postgraduate student, Department of General Physics, Voronezh State University (Voronezh, Russian Federation).

https://orcid.org/0000-0003-2597-3602
pisliaruk@phys.vsu.ru

Evelina P. Domashevskaya, Dr. Sci. (Phys.–Math.), Professor, Consulting Professor, Department of Solid State Physics and Nanostructures, Voronezh State University (Voronezh, Russian Federation).

https://orcid.org/0000-0002-6354-4799
ftt@phys.vsu.ru

Received August 12, 2025; approved after reviewing September 17, 2025; accepted for publication October 15, 2025; published online April 01, 2026.